Recent Progress in Polarization Enhanced PVDF Based Perovskite Solar Cells

Jiaheng Nie [1], Yaming Zhang [2], Jizheng Wang [3], Lijie Li [4], and Yan Zhang [2,*]

[1] *School of Cybersecurity, Chengdu University of Information Technology, Chengdu 610225, China*

[2] *School of Physics, University of Electronic Science and Technology of China, Chengdu 610054, China*

[3] *Beijing National Laboratory for Molecular· Sciences, CAS Key Laboratory of Organic Solids, Institute of Chemistry, Chinese Academy of Sciences, Beijing 100190, China*

[4] *College of Engineering, Swansea University, Swansea SA1 8EN, UK*

[*] To whom correspondence should be addressed, E-mail: zhangyan@uestc.edu.cn

Abstract

PVDF-based perovskite solar cells have led to continuous improvements in efficiency of up to 24.23% [1]. This type of polarization enhanced solar cells offers a simpler strategy to achieve stable polarization to increase efficiency. We review the fundamental research progress in polarization-enhanced built-in field in PVDF-based perovskite solar cells. We discuss how polarization can be induced by piezo-phototronic effect, spontaneous and external electric field poling. Finally, we outline directions for high-efficiency perovskite solar cells based on PVDF.

Keywords: piezo-phototronics; perovskite solar cell; polarization; surface potential.

1. Introduction

Perovskite solar cells (PSCs) have shown promising in photovoltaic power generation due to their excellent optoelectronic and material properties such as high absorption coefficient [2-4], low exciton binding energy [5-7], and long carrier diffusion lengths [8-10], which represent a highly efficient alternative to fossil fuels. The low-cost fabrication steps and impressive performance of PSC demonstrate the potential for rapid industrial realization [11-13]. The rapid efficiency breakthrough to over 25.7% in just over a decade rivals the progress of traditional silicon solar cells over several decades [14]. Based on the Shockley-Queisser or radiative limit, theoretical maximum efficiency of ~33% for single-junction perovskite solar cells [15]. There are still significant room for further increasing the power conversion efficiency (PCE) of cells by reducing energy loss during the photoelectric conversion [16-19].

Many methods have been developed to improve device performance by decreasing energy loss [20-26], which can be divided into two categories: One category is to increase efficiency by tuning the physical functionalities of the device, which change the potential internal device for improving PCE through physical stimuli such as applied strain, and electric fields [20, 21, 27, 28]. Wang's group constructed a piezo-phototronic solar cell with a metal-semiconductor junction structure based on Cu2S/CdS coaxial nanowires, which improved the device efficiency by utilizing piezo-potential induced by external strain [29]. Based on the piezo-phototronic effect, strain-induced polarization in flexible perovskite solar cells increase built-in field of perovskite solar cells, improving the PCE of flexible PSCs by 40% [20]. Yang et al. have reported an applied electric field induced a permanent internal electric field of 50 V/μm in ferroelectric polymers, which can enhance the built-in field (BIF) in organic solar cells, achieves an improvement of 10% - 20% in the efficiency of organic solar cell devices compared to other methods [30]. Due to polarization of PVDF-based materials by electric poling, molecular dipole orientations can be turned by external electric fields. This ordered polarization can induce a permanent internal electric field of 50 V/μm, superposing with the built-in field of the cell to form a stronger driving force, increasing photocurrent generation by reducing recombination and raising the device V_{OC} by maintaining high quasi-Fermi levels of electrons [30]. The polarization of PVDF-based materials can increase carrier drift length, prolong carrier

lifetime before recombination, and enhance carrier collection efficiency. The other category is to minimize energy loss by adjusting the chemical reactions during perovskite formation or device operation, including solvent engineering [31], compositional engineering [32], defect engineering [33]. PVDF-based materials can be used as dopants in photoactive perovskite layers to modulate perovskite crystallization kinetics [34]. By establishing stable hydrogen bonds with perovskites, PVDF-based materials strengthen the tension force of grains, promoting the formation of larger grains and a more compact morphology in the films. The polarization of PVDF-based materials can also guide the ordered growth of perovskites, reducing nucleation sites and defects in the perovskite films. PVDF-based materials facilitate high-quality perovskite film formation, effectively reducing recombination losses induced by defects and trap states in the films, enhancing the optoelectronic properties of the films, and thereby improving device efficiency.

Energy loss is induced by internal nonradiative recombination at the absorption layer or interface [35]. The energy loss is expressed as $E_{loss} = E_g - eV_{oc}$, where E_g is the optical bandgap of perovskite, V_{OC} is the open-circuit voltage [36-38]. There are most of energy loss related to defect trapping, charge accumulation, interface matching or crystallization of perovskite, limit efficiency of PSCs [39-42]. In this manuscript, we reviewed the impacts of strain, external electric fields or strain on the built-in fields of solar cells, then analyzed the mechanisms of polarization effects on built-in fields, and finally looked ahead to the influences of polarization on interfacial barriers in the cells. We then summarize the prospects and challenges for large-scale application of polarization-enhanced perovskite solar cells, and provide several possible approaches for developing strategies to polarization enhancement of perovskite solar cells.

2. Strain-induced polarization enhanced perovskite solar cells by piezo-phototronic effect

Piezotronic and piezo-phototronic effect use strain-induced polarization to improve the efficiency of solar cells, which provide a simple and effective approach for high-performance solar cells. The piezo-phototronic effect utilizes polarization to increase built-in electric field and control carrier transport, coupling of semiconductors, photo-excitation, and polarization

[43-45]. It has wide applications in areas including transistors, photodetectors, solar cells, and LEDs [46-52]. Piezotronic and piezo-phototronic effect can be effective strategy to minimize energy loss of perovskite solar cells.

Zhu et al. designed a silicon-based solar cell with a heterojunction structure of ZnO and Si, which utilizes the piezoelectric polarization generated in ZnO nanowires under strain to enhance the transport of photogenerated carriers in the device, increasing the efficiency to 9.51% [53]. The piezo-phototronic effect utilizes the polarization induced by strain to modulate the band structure at the interface between ZnO and PbS-quantum dots, as well as control the depletion width in the quantum dot layer, enabling efficient carrier extraction [54]. Under -0.25% compressive strain, the efficiency was significantly enhanced by about 30%. The enhancement of built-in fields and modulation of carrier separation and transport by the piezo-phototronic effect are important for engineering the design of perovskite solar cell structures to further improve efficiency. Understanding the mechanism of how the polarization induced by the piezo-phototronic effect influences perovskite solar cell devices, and guiding the design for highly efficient and stable PSCs, are crucial for the further large-scale application of perovskite solar cells.

Sun et al. presented a strategy to improve the efficiency of flexible perovskite solar cell devices through strain, by growing a layer of ZnO nanowire array as the electron transport layer of the solar cell, forming a heterojunction with the perovskite, as shown in Fig. 1 [20]. When strain is applied on the ZnO nanowires, the piezoelectric potential generated at the two ends of the ZnO nanowires can modulate the built-in field and energy band structure of the heterojunction interface in the device. When the solar cell is bent upward, strain-induced positive piezoelectric potential is generated at the heterojunction interface, increasing the built-in field and decreasing interface barriers. When the device is bent downward, negative piezoelectric potential is generated at the heterojunction interface, decreasing the built-in field and increasing interface barriers.

Hu et al. fabricated flexible ZnO/perovskite solar cells based on single ZnO microwires and investigated the influence of strain-induced polarity in ZnO on device performance, as shown in Fig. 2 [55]. The influence of strain-induced polarization on device performance was experimentally and systematically studied by applying continuously adjustable strain. The

results demonstrated that -0.8% compressive strain increased the V_{OC} of the device from 0.59 V to 0.74 V, while 0.71% tensile strain decreased the V_{OC} of the device from 0.73 V to 0.7 V.

3. Polarization improves built-in field by external electric field poling

Energy loss in perovskite solar cells originates from recombination, including non-radiative recombination at interfaces and within the perovskite layer [56-58]. Doping or incorporating ferroelectric polymers internally or as interfacial layers enhances the built-in field, reducing non-radiative recombination in devices [30, 34, 59]. Perovskite films doped with ferroelectric polymers exhibited ordered alignment of organic cations, reduced trap states during film formation, and facilitated high quality film growth. The polarization of ferroelectric polymers induced by the external electric field broadens the depletion region, playing a critical role in enhancing the built-in field.

The built-in field, as a main driving force, make the carriers to drift to corresponding electrodes, avoiding recombination. A weak BIF cannot provide insufficient driving force, and makes holes and electrons be either captured by charged defect or accumulate at the interface [30, 60]. Although applying an external electric field to the perovskite layer can enhance BIF of device and reduce carrier recombination at charged defect [61, 62]. The polarization by only external electric field is easily screened by the ion migration or accumulation after storing for some time. ferroelectric polymers as a group of polar materials can offer stable and controllable additional electric field in PSCs, by maintain a permanent electric polarization [63-67].

P(VDF-TrFE), P(VDF-TrFE-CFE), P(VDF-TrFE-CTFE), as typical ferroelectric polymers, owning different remnant polarization and coercive electric fields is PVDF-based organic ferroelectric polymers, can be doped in perovskite layers to enhance BIF, due to its solution processability. Yang et al. developed a strategy to remain stable polarization via the combination of doping these three ferroelectric polymers and poling by external electric field [21], as shown in Fig. 3. The external electronic field is applied on the ferroelectric polymer doped films at bottom FTO substrate and an additional top FTO conductive glass. The built-in potential (V_{bi}) in the PSCs, is measured by Mott–Schottky analysis and visualized by Kelvin probe force microscopy (KPFM), to explain how the ferroelectric polymers have an influence on cell performance. Mott–Schottky and

KPFM characteristic shows an additional potential of about 0.2 V after doping P(VDF-TrFE). Introducing ferroelectric polymer did provide an additional electric field to enhance the V_{bi}. Figure 3(b) shows the PCE in the condition of ferroelectric polymer doping, only external electric field treatment and the ferroelectric polymer polarization. Because of synergistic effects, the ferroelectric polymer-based PSCs after electric field poling show a high PCE of 21.38% with a V_{OC} of 1.14 V.

4. Spontaneous polarization improves built-in field

Although selective doping can easily enhance the BIF in silicon-based solar cells to obtain high performance [68-70], it is difficult to achieve controllable doping to readily boost the BIF in perovskite solar cells [1]. The polarization of a high polarization organic polymer PVDF:DH can be driven by BIF of the device, forming a permanently sustained electric field inside the device to enhance the built-in field, effectively driving carrier transport and extraction, reducing internal recombination. Meanwhile, PVDF:DH enables the PbI_2 precursor solution to form a mesoporous film, facilitating effective incorporation with the ammonium salt solution, improving film crystallinity, and reducing in-layer defects.

When the external electric field is lower than the coercive electric field of the ferroelectric polymers, it is difficult to maintain the polarization orientation without the external electric field [71-73]. However excessively high electric field intensity will damage the device [74]. To form a stable polarization, it is important to tune the external electric field intensities below dielectric breakdown strengths of PSC devices and above the coercive electric field. There is a big difficulty to exactly calculate the applied external voltage of the per-unit-thickness and achieve such a small repeatable field.

Chen et al. carried out a feasible strategy to keep permanently contribution of ferroelectric polymers to BIF, by doping PVDF-DH polymer with high polarizability without external electric field poling [75]. Polarization of ferroelectric polymer can be driven by the BIF of the PSC itself. An additional electric field induced by polarized ferroelectric polymer is permanent [71, 76]. Due to the direction of this field is consistent with that of BIF of PSC itself, polarization of doped PVDF-DH enhances the BIF in the device. It is easy to polarize PVDF:DH using electric field poling, because the hydrogen bonding interaction between the F atom of PVDF and the N-H bond in DH

induce the all-trans arrangement of CH_2CF_2 in PVDF [77-81]. The polarization of PVDF:DH can be driven by BIF, showing a consistent vector direction to that of external electric field poling. Figure 4(a) shows increased potential of perovskite layer measured by KPFM, by depositing the perovskite film on the ETL for simulate a real PSC, indicating that V_{bi} increase after doping ferroelectric polymer [82]. Mott–Schottky fitting further shows the V_{bi} increase from 1.01 V without PVDF:DH dopant to 1.07 V with PVDF:DH dopant. Figure 4(b) shows plausible mechanism of polarization of PVDF:DH driven by BIF itself instead of external electric field enhancing BIF. The DH in the PVDF:DH drives PVDF molecules into an all-trans arrangement, due to the existence of hydrogen bonding between PVDF and DH. The oriented PVDF:DH is polarized by BIF toward the upward, produce an additional electric field with the direction consistent with that of the BIF of device. So, the BIF is enhanced by the electric field superposition, facilitates charge-carrier transport and extraction, and increase the V_{OC} of PSCs. Compared to PSCs without doping ferroelectric polymers (1-control devices), The target device doped ferroelectric polymers remain the almost same V_{OC} after external electric field poling for 12 h, as shown in Fig. 4(c). The resulting devices show an efficiency of 24.23% (0.062 cm^2 device) with V_{OC} of 1.16 V. and an efficiency of 22.69% with a larger area of 1 cm^2.

The efficiency of perovskite solar cells still is far behind the theoretical limit, mainly due to open-circuit voltage losses caused by grain boundary defects in solution-processed perovskite solar cells acting as recombination centers. The ferroelectric polymer PVDF can form strong hydrogen bonding interactions with perovskites, optimizing the grain growth process, effectively passivating defects, significantly decreasing non-radiative recombination losses, and minimizing open-circuit voltage losses.

Because of high energy loss in V_{OC}, there is much room to maximize the efficiency of perovskite solar cells. Most of the energy loss in PSCs are still remained in the range of 0.33 to 0.40 eV, though enhancing device performance by optimizing additives [83-85], deposition methods [86-89], or tuning composition [41, 85]. Increasing V_{OC} can further promote PCE of device. There are abundant structural defects at the grain boundaries of the polycrystalline perovskite films deposited

by solution processes [90]. The defect states of films can lead to energy loss and reductions in V_{OC}. And charged defects inducing the deep-level traps, can serve as non-radiative recombination centers, limiting the final efficiency of PSCs [91, 92]. Among the PSCs parameters, non-radiative recombination has most influence on V_{OC} [93, 94]. Doping ferroelectric polymers can form continuously perovskite–polymer composite ordering by establishing stable interactions, for reducing recombination.

It is essential to reduce energy loss induced by non-radiative channels and increase V_{OC} for further improving device PCE. Sun et al. introducing PVDF polymers in perovskite material to form high-quality perovskite layer for decreasing energy loss of V_{OC} [95]. Hydrogen-bonds are formed by the F atoms of PVDF reacting with organic cation (MA^+ or FA^+) and coordinate bonds of Pb^{2+} in perovskite, during the fabrication process, reducing charged defect of film. PVDF also act as connecting bridge grain boundaries to passivate vacancies of organic cation and halide anion, for inhibiting non-radiative recombination and decrease loss of V_{OC}. Figure 5 shows PVDF-doped PSCs with an attractive high V_{OC} of 1.22 V, achieving 96% of the S–Q limit V_{OC} (1.27 V) at the absorption threshold of 1.55 eV. It is one of the highest V_{OC} values in $FAMAPb(I/Br)_3$ solar cells. The increase of V_{OC} induced by the better crystallization of perovskite and effective passivation effect of the F-atoms of PVDF in perovskite. The V_{bi} of PVDF-based PSCs measured by Mott–Schottky characteristic, achieve to 1.04 V higher than 0.94 V of PSCs without doping PVDF. The enhcanced V_{bi} can increase V_{OC} of PSCs, facilitate carrier transport and reduce carrier recombination. The strong interaction between perovskite and PVDF minimize Losses of V_{OC}, makes $FAMAPb(I/Br)_3$-based PSCs achieve a PCE of 24.21 % with V_{OC} of 1.22 V.

5. Polarized molecular improves built-in field by external field poling

Non-radiative recombination of carriers is an important cause of energy loss in perovskite solar cells [96, 97]. Enhancing the built-in field or passivating defects can facilitate effective carrier separation, minimizing energy loss [98-100]. Homochiral ferroelectrics with ionic structures similar

to perovskites can effectively reduce the density of electronic trap states in the perovskite layer, decreasing open-circuit voltage losses [101].

Ferroelectric polymers can present a switched polarization orientation to keep permanent electric field with external electric field poling, is considered to be one of the most important materials to increase V_{OC} [102-104]. Molecular ferroelectric polymers emerged as an attractive ferroelectric family, present a remarkable ferroelectric response comparable to ferroelectric polymers, and the properties of easy and environment-friendly fabrication, low preparation temperature and flexibility [105-109]. Introducing this homochiral molecular ferroelectric polymers can enlarge the BIF of solar cells and passivate charge defect due to the similarities in ionic structure.

Xu et al chosen molecular FE material as dopant to construct PSCs with high V_{OC} [110]. The electron–hole nonradiative recombination deceases by chemical tailoring of the ionic structures with filling iodide vacancies and cation exchange.[111]. Molecular ferroelectric polymers shows high spontaneous polarization intensity of 13.96 μC cm^{-2} at 293 K, superior to some inorganic perovskite ferroelectrics [112]. Figure 6(a) shows the device structures of PSCs and schematic of ideal carriers separation process after electric field poling. Employing molecular ferroelectric polymers enlarge BIF as transporting driving force to suppress deep level defects and achieve more efficient charge separation after external electric field poling. AFM morphology and the corresponding surface contact potential difference (CPD) at the interfaces of TiO_2 and perovskite layers is shown in Fig. 6(b). CPD value of molecular ferroelectric polymers doped perovskite/TiO_2 is higher than that of control film/TiO_2. Polarization of molecular ferroelectric polymers increase the BIF of perovskite solar cells. Figure 6(c) characterizes the performance of molecular ferroelectric polymers doped PSCs in the condition of different electric field poling conditions. The average PCEs of PSCs under the electric fields increasing from 0 to 1 V/μm for 5 min increase, while the electric fields above 1 V/μm decrease the PCE of device by burning the structure of PSCs. Compared to device without electric field poling. applying positive electric field poling improves performance of the PSCs and applying negative electric field poling reduces performance of the PSCs. The performance measurement of PSCs also improves with poling time, and achieve to maximun at the poling time of 5 minutes, due to the polarization reaches saturation state. The photovoltaic molecular ferroelectric polymers PSCs achieves a power conversion efficiency as high as 21.78 %.

6. High orderly polarizated ferroelectric polymer improves built-in field of perovskite solar cells

Pure organic-inorganic hybrid perovskite films showed no significant piezoresponse, while perovskite films doped with ferroelectric polymers exhibited ferroelectricity [1]. The polarization of the ferroelectric thin films induced by applied bias can effectively facilitate charge extraction, reduce recombination losses, and prolong minority carrier lifetimes [113-115]. Regulating the orderly polarization of the ferroelectric polymers allows tunable photovoltaic performance of the devices [116].

The ferroelectric polymer not only has proven to increase the carriers separation, transfer, extraction and collection efficiency in ferroelectric photovoltaic devices [30, 65, 66, 117, 118], but also promote the crystallinity of films and the passivation at the grain boundary[119, 120]. Furthermore, high orderly polarization induced by external electric field can turn V_{OC} and performance of PSCs by form permanent electric field [21, 30, 75].

Jia et al. fabricated perovskite solar cells of enhanced performance, by incorporating permanent electric field induced by poling and ferroelectric copolymer dopant P(VDF-TrFE) [81]. Figure 7(a) shows the influence of the electric field poling process on cell efficiency with 2 wt% P(VDF-TrFE). The ferroelectric films are applied by external bias of 5 V and 10 V for 10 mins. The performance characteristics device is measured after depositing HTL and Au electrodes. Applying a positive electric field poling will active P(VDF-TrFE) doped perovskite layer, make polarization orientation of P(VDF-TrFE) have the same direction as BIF of the p–i–n junction. The positive electric field poling increases the V_{OC} from about 1.05 V to about 1.15 V. To maximize efficiency of $MAPbI_3$ PSCs also need to optimize concentration of P(VDF-TrFE), for the trade-off among the enhancing build-in field, increasing series resistance, and decreasing pinholes induced by extra roughness. The optimized doping concentration of P(VDF-TrFE) was ≈ 0.5 wt%, and can increase the V_{OC} by about 0.11 V, due to the partial spontaneous polarization of the P(VDF-TrFE). The average V_{OC} of the PSCs with ferroelectric polymer achieved a value of over 1.17 V, by further applying electric field poling. And the highest V_{OC} value reached 1.174 V compared to 1.05 V without poling

process. The mechanism of influence of electric field poling on V_{OC} was drawn in Fig. 7(c). When Appling positive poling, an additional electric induced by high orderly polarization of P(VDF-TrFE) is calculated to be 20 V/μm, much higher than BIF of cells calculated to less than 1.5 V/μm. Enhanced BIF can not only extend width of depletion layer to increase V_{OC} of PSCs, but also decrease the probability of recombination and increase carrier lifetime to reduce recombination. Appling negative poling can weaken the influence of BIF, increase carrier recombination, and lead to lower V_{OC}. High orderly polarization induced by external field poling increase PCF by 30% for MAPbI3 perovskite solar cell.

7. Mechanism of built-in field enhanced by polarization

Due to Auger recombination, band tail recombination, or interface recombination, the V_{OC} of solar cells is evidenced to be below the S-Q limiting value [121-123]. A sufficient built-in field strength can effectively suppress recombination losses and increase the V_{OC} of the device [124-126]. The electric field generated by polarization induced through applied electric fields or strain can enhance the built-in field of the cells. To investigate the physical mechanisms of the polarization enhanced cells performance after electric fields poling or strain, the energy band diagrams tuned by polarization were shown in Fig. 8.

Figure 8(a) shows the potential distribution map of the cross-section of the p-i-n structured perovskite solar cells under dark and light illumination conditions. After light illumination, an obvious unbalanced potential is generated internally in the device, leading to the formation of a built-in field. Figure 8(b) displays the band alignment of the solar cells before contact, under dark conditions, and under light illumination. Under illumination, the conduction and valence bands shift, and a built-in field is generated in the device. Figure 8(c) shows the overall energy band diagram of a PSCs under different polarization. The positive polarization formed an additional electric field aligned with the built-in field, causing holes to drift rapidly to the interface between the perovskite layer and the hole transport layer, and electrons to drift to the interface between the perovskite layer and electron transport layer. The charge accumulation at the interfaces induced band bending in the p-i-n structure, enhancing the V_{OC} of the device.

In contrast, negative polarization induced an electric field in opposite direction, which can lead to insufficient driving force for internal carriers to reach the interface, resulting in extensive recombination internally. Meanwhile, the reduced interfacial charge affects band bending, decreasing V_{OC} of cells. The local electric field induced by polarization provide a stable field for enhancing built-in field, and provide a sufficient electric field force to promote more carrier separation, transport process, reducing recombination loss of carriers. Polarization induced by piezo-phototronic effect provide a promising approach for further improving cells performance, by increasing energy collection efficiency.

8. Challenges for future perovskite solar cells enhanced by polarization

In this review, external electric fields poling used for increasing V_{OC} and enhancing efficiency and polarization enhanced mechanism are reviewed. The polarization of the ferroelectric polymer induced by strain or external electric field allows an additional electric field to add on the built-in field. Thus, the methods of external field poling allow the further performance enhancement without destroying device, after device preparation. Although polarization induced by external field poling increase PCE of devices, there are still some challenges that need to be addressed in this research area.

1. KPFM can characterize the internal potential distribution of devices, and has been utilized to observe increased interfacial potentials by doping with ferroelectric polymers. The cross-sectional potential distribution of perovskite devices after polarization under an applied electric field can be directly examined using KPFM, elucidating the impacts of positive and negative polarization on the interfacial potentials of perovskite solar cells.

2. The polarization of ferroelectric polymers results in high quality perovskite thin films, due to the strong hydrogen bonding interactions during the fabrication process. The polarization can potentially influence the electrochemical reactions associated with perovskite formation by modulating the charge transfer process, for promoting the generation of larger perovskite crystals.

3. Experiments have studied the impacts of positive and negative polarization of ferroelectric (FE) polymers on device performance. Further research needs to investigate the

mechanisms of how the angle between the polarization orientation and built-in field direction affects device performance. In addition to the role of built-in fields, the influence of interfacial barriers on device performance is also very important.

4. The permanent polarization of ferroelectric polymers induced by the external electric field can potentially modulate interfacial barriers by influencing the interfacial potential distribution, promoting effective carrier injection, and impacting device performance. Experiments can investigate the effects of polarization on the uniformity of perovskite thin film surface potential by comparing the surface energy states before and after polarization.

PVDF-based materials can be used as dopants in the perovskite layer owing to their chemical stability and solution processability, improving the nucleation and growth of perovskite crystals, modulating defect states and crystallization kinetics in the films to enhance the quality of perovskite films. The abundant F atoms in PVDF-based materials can react with H atoms to form F-H bonds, guiding crystal orientation and phase structure formation during the perovskite formation process. As organic ferroelectric materials, PVDF-based materials possess strong polarization characteristics. The polarization induced by external electric fields or spontaneous polarization of the materials themselves can enhance the internal electric field in perovskite solar cells, improving carrier transport efficiency. The dipoles in the materials can also tune the energy levels on the perovskite surface, modulate interfacial energy levels, and facilitate carrier injection. The hydrophobicity of PVDF-based materials can effectively prevent perovskite decomposition caused by water molecule ingress, enhancing device stability. The synergistic effects of PVDF-based materials are remarkable in optimizing perovskite quality, tuning interfacial energetics, and preventing device degradation. This provides a promising strategy to minimize non-radiative recombination losses of perovskites layer or interfaces, and to prevent perovskite decomposition, thereby enhancing device efficiency and stability. Meanwhile, this strategy paves new way for large-scale fabrication and tuning of perovskite solar cells, and also promote the development of other advanced thin-film optoelectronic devices.

Acknowledgments

The authors are thankful for support from Major Program of National Natural Science Foundation of China (Grant No. 52192610, 52192612) and Key Program of National Natural Science Foundation of China (Grant No. U22A2077). The authors are thankful for the support by the Fundamental Research Funds for the Central Universities (grant no. ZYGX2021YGCX001).

Credit authorship contribution statement

Jiaheng Nie: Methodology, Formal analysis, Data curation, Writing- original draft, Validation; **Yaming Zhang:** Formal analysis, Writing- original draft; **Jizheng Wang:** Formal analysis, Writing-review & editing; **Lijie Li:** Formal analysis, Writing-review & editing; **Yan Zhang:** Supervision, Conceptualization, Methodology, Formal analysis, Writing-review & editing.

Competing interests

The authors declare no competing interests.

References

[1] W. Chen, S. Liu, Q. Li, Q. Cheng, B. He, Z. Hu, Y. Shen, H. Chen, G. Xu, X. Ou, H. Yang, J. Xi, Y. Li, Y. Li, Adv. Mater., 34 (2022) 2110482.

[2] J. De Roo, M. Ibáñez, P. Geiregat, G. Nedelcu, W. Walravens, J. Maes, J.C. Martins, I. Van Driessche, M.V. Kovalenko, Z. Hens, ACS Nano, 10 (2016) 2071-2081.

[3] J.-H. Im, C.-R. Lee, J.-W. Lee, S.-W. Park, N.-G. Park, Nanoscale, 3 (2011) 4088-4093.

[4] N.-G. Park, Mater. Today, 18 (2015) 65-72.

[5] A. Miyata, A. Mitioglu, P. Plochocka, O. Portugall, J.T.-W. Wang, S.D. Stranks, H.J. Snaith, R.J. Nicholas, Nat. Phys., 11 (2015) 582-587.

[6] K. Galkowski, A. Mitioglu, A. Miyata, P. Plochocka, O. Portugall, G.E. Eperon, J.T.-W. Wang, T. Stergiopoulos, S.D. Stranks, H.J. Snaith, R.J. Nicholas, Energy Environ. Sci., 9 (2016) 962-970.

[7] V. D'Innocenzo, G. Grancini, M.J.P. Alcocer, A.R.S. Kandada, S.D. Stranks, M.M. Lee, G. Lanzani, H.J. Snaith, A. Petrozza, Nat. Commun., 5 (2014) 3586.

[8] D. Shi, V. Adinolfi, R. Comin, M. Yuan, E. Alarousu, A. Buin, Y. Chen, S. Hoogland, A. Rothenberger, K. Katsiev, Y. Losovyj, X. Zhang, P.A. Dowben, O.F. Mohammed, E.H. Sargent, O.M. Bakr, Science, 347 (2015) 519-522.

[9] Z. Yang, Z. Yu, H. Wei, X. Xiao, Z. Ni, B. Chen, Y. Deng, S.N. Habisreutinger, X. Chen, K. Wang, J. Zhao, P.N. Rudd, J.J. Berry, M.C. Beard, J. Huang, Nat. Commun., 10 (2019) 4498.

[10] Z. Guo, J.S. Manser, Y. Wan, P.V. Kamat, L. Huang, Nat. Commun., 6 (2015) 7471.

[11] N.J. Jeon, J.H. Noh, W.S. Yang, Y.C. Kim, S. Ryu, J. Seo, S.I. Seok, Nature, 517 (2015) 476-480.

[12] J.J. Yoo, G. Seo, M.R. Chua, T.G. Park, Y. Lu, F. Rotermund, Y.-K. Kim, C.S. Moon, N.J. Jeon, J.-P. Correa-Baena, V. Bulović, S.S. Shin, M.G. Bawendi, J. Seo, Nature, 590 (2021) 587-593.

[13] Y. Rong, Y. Hu, A. Mei, H. Tan, M.I. Saidaminov, S.I. Seok, M.D. McGehee, E.H. Sargent, H. Han, Science, 361 (2018) eaat8235.

[14] J. Park, J. Kim, H.-S. Yun, M.J. Paik, E. Noh, H.J. Mun, M.G. Kim, T.J. Shin, S.I. Seok, Nature, 616 (2023) 724-730.

[15] S. Albrecht, B. Rech, Nat. Energy, 2 (2017) 1-2.

[16] M. Stolterfoht, C.M. Wolff, J.A. Márquez, S. Zhang, C.J. Hages, D. Rothhardt, S. Albrecht, P.L. Burn, P. Meredith, T. Unold, D. Neher, Nat. Energy, 3 (2018) 847-854.

[17] D. Qian, Z. Zheng, H. Yao, W. Tress, T.R. Hopper, S. Chen, S. Li, J. Liu, S. Chen, J. Zhang, X.K. Liu, B. Gao, L. Ouyang, Y. Jin, G. Pozina, I.A. Buyanova, W.M. Chen, O. Inganas, V. Coropceanu, J.L. Bredas, H. Yan, J. Hou, F. Zhang, A.A. Bakulin, F. Gao, Nat Mater, 17 (2018) 703-709.

[18] Q. Zeng, X. Zhang, X. Feng, S. Lu, Z. Chen, X. Yong, S.A.T. Redfern, H. Wei, H. Wang, H. Shen, W. Zhang, W. Zheng, H. Zhang, J.S. Tse, B. Yang, Adv Mater, 30 (2018) 1705393.

[19] L. Yan, Q. Xue, M. Liu, Z. Zhu, J. Tian, Z. Li, Z. Chen, Z. Chen, H. Yan, H.L. Yip, Y. Cao, Adv Mater, (2018) e1802509.

[20] J. Sun, Q. Hua, R. Zhou, D. Li, W. Guo, X. Li, G. Hu, C. Shan, Q. Meng, L. Dong, C. Pan, Z.L. Wang, ACS Nano, 13 (2019) 4507-4513.

[21] C.C. Zhang, Z.K. Wang, S. Yuan, R. Wang, M. Li, M.F. Jimoh, L.S. Liao, Y. Yang, Adv Mater, 31 (2019) e1902222.
[22] R. Lin, J. Xu, M. Wei, Y. Wang, Z. Qin, Z. Liu, J. Wu, K. Xiao, B. Chen, S.M. Park, G. Chen, H.R. Atapattu, K.R. Graham, J. Xu, J. Zhu, L. Li, C. Zhang, E.H. Sargent, H. Tan, Nature, 603 (2022) 73-78.
[23] H. Min, D.Y. Lee, J. Kim, G. Kim, K.S. Lee, J. Kim, M.J. Paik, Y.K. Kim, K.S. Kim, M.G. Kim, T.J. Shin, S. Il Seok, Nature, 598 (2021) 444-450.
[24] G. Yang, Z. Ren, K. Liu, M. Qin, W. Deng, H. Zhang, H. Wang, J. Liang, F. Ye, Q. Liang, H. Yin, Y. Chen, Y. Zhuang, S. Li, B. Gao, J. Wang, T. Shi, X. Wang, X. Lu, H. Wu, J. Hou, D. Lei, S.K. So, Y. Yang, G. Fang, G. Li, Nature Photonics, 15 (2021) 681-689.
[25] M. Kim, J. Jeong, H. Lu, T.K. Lee, F.T. Eickemeyer, Y. Liu, I.W. Choi, S.J. Choi, Y. Jo, H.B. Kim, S.I. Mo, Y.K. Kim, H. Lee, N.G. An, S. Cho, W.R. Tress, S.M. Zakeeruddin, A. Hagfeldt, J.Y. Kim, M. Gratzel, D.S. Kim, Science, 375 (2022) 302-306.
[26] Z. Li, B. Li, X. Wu, S.A. Sheppard, S. Zhang, D. Gao, N.J. Long, Z. Zhu, Science, 376 (2022) 416-420.
[27] E. Jia, D. Wei, P. Cui, J. Ji, H. Huang, H. Jiang, S. Dou, M. Li, C. Zhou, W. Wang, Adv Sci (Weinh), 6 (2019) 1900252.
[28] J. Nie, Y. Zhang, M. Dan, J. Wang, L. Li, Y. Zhang, Sol. RRL, 5 (2021) 2100692.
[29] C. Pan, S. Niu, Y. Ding, L. Dong, R. Yu, Y. Liu, G. Zhu, Z.L. Wang, Nano Lett, 12 (2012) 3302-3307.
[30] Y. Yuan, T.J. Reece, P. Sharma, S. Poddar, S. Ducharme, A. Gruverman, Y. Yang, J. Huang, Nat Mater, 10 (2011) 296-302.
[31] N.J. Jeon, J.H. Noh, Y.C. Kim, W.S. Yang, S. Ryu, S.I. Seok, Nat Mater, 13 (2014) 897-903.
[32] N.J. Jeon, J.H. Noh, W.S. Yang, Y.C. Kim, S. Ryu, J. Seo, S.I. Seok, Nature, 517 (2015) 476-480.
[33] D.Y. Son, S.G. Kim, J.Y. Seo, S.H. Lee, H. Shin, D. Lee, N.G. Park, J Am Chem Soc, 140 (2018) 1358-1364.
[34] C.C. Zhang, Z.K. Wang, S. Yuan, R. Wang, M. Li, M.F. Jimoh, L.S. Liao, Y. Yang, Adv. Mater., (2019) 1902222.
[35] D. Luo, R. Su, W. Zhang, Q. Gong, R. Zhu, Nature Reviews Materials, 5 (2019) 44-60.
[36] L. Xie, J. Liu, J. Li, C. Liu, Z. Pu, P. Xu, Y. Wang, Y. Meng, M. Yang, Z. Ge, Adv Mater, (2023) e2302752.
[37] S.M. Menke, N.A. Ran, G.C. Bazan, R.H. Friend, Joule, 2 (2018) 25-35.
[38] P. Cheng, M. Zhang, T.K. Lau, Y. Wu, B. Jia, J. Wang, C. Yan, M. Qin, X. Lu, X. Zhan, Adv Mater, 29 (2017) 1605216.
[39] J. Ma, G. Yang, M. Qin, X. Zheng, H. Lei, C. Chen, Z. Chen, Y. Guo, H. Han, X. Zhao, G. Fang, Adv Sci (Weinh), 4 (2017) 1700031.
[40] E.H. Jung, B. Chen, K. Bertens, M. Vafaie, S. Teale, A. Proppe, Y. Hou, T. Zhu, C. Zheng, E.H. Sargent, ACS Energy Letters, 5 (2020) 2796-2801.
[41] S. Wu, J. Zhang, Z. Li, D. Liu, M. Qin, S.H. Cheung, X. Lu, D. Lei, S.K. So, Z. Zhu, A.K.Y. Jen, Joule, 4 (2020) 1248-1262.
[42] B. Zhao, M. Abdi-Jalebi, M. Tabachnyk, H. Glass, V.S. Kamboj, W. Nie, A.J. Pearson, Y. Puttisong, K.C. Godel, H.E. Beere, D.A. Ritchie, A.D. Mohite, S.E. Dutton, R.H. Friend,

A. Sadhanala, Adv Mater, 29 (2017) 1604744.
[43] Y. Zhang, Y. Leng, M. Willatzen, B. Huang, MRS Bulletin, 43 (2018) 928-935.
[44] Y. Zhang, Y. Yang, Z.L. Wang, Energy & Environmental Science, 5 (2012) 6850-6856.
[45] W. Wu, Z.L. Wang, Nature Reviews Materials, 1 (2016) 1-17.
[46] C. Pan, L. Dong, G. Zhu, S. Niu, R. Yu, Q. Yang, Y. Liu, Z.L. Wang, Nature Photonics, 7 (2013) 752-758.
[47] L. Zhu, Z.L. Wang, Advanced Functional Materials, 29 (2018) 1808214.
[48] M. Peng, Y. Liu, A. Yu, Y. Zhang, C. Liu, J. Liu, W. Wu, K. Zhang, X. Shi, J. Kou, J. Zhai, Z.L. Wang, ACS Nano, 10 (2016) 1572-1579.
[49] C. Pan, M. Chen, R. Yu, Q. Yang, Y. Hu, Y. Zhang, Z.L. Wang, Adv Mater, 28 (2016) 1535-1552.
[50] Z.L. Wang, Adv Mater, 24 (2012) 4632-4646.
[51] L. Pan, S. Sun, Y. Chen, P. Wang, J. Wang, X. Zhang, J.J. Zou, Z.L. Wang, Advanced Energy Materials, 10 (2020) 2000214.
[52] L. Zhu, L. Wang, F. Xue, L. Chen, J. Fu, X. Feng, T. Li, Z.L. Wang, Adv Sci (Weinh), 4 (2017) 1600185.
[53] L. Zhu, L. Wang, C. Pan, L. Chen, F. Xue, B. Chen, L. Yang, L. Su, Z.L. Wang, ACS Nano, 11 (2017) 1894-1900.
[54] J. Shi, P. Zhao, X. Wang, Adv. Mater., 25 (2013) 916-921.
[55] G. Hu, W. Guo, R. Yu, X. Yang, R. Zhou, C. Pan, Z.L. Wang, Nano Energy, 23 (2016) 27-33.
[56] C.M. Wolff, P. Caprioglio, M. Stolterfoht, D. Neher, Adv. Mater., 31 (2019) 1902762.
[57] J. Wang, J. Zhang, Y. Zhou, H. Liu, Q. Xue, X. Li, C.-C. Chueh, H.-L. Yip, Z. Zhu, A.K.Y. Jen, Nat. Commun., 11 (2020) 177.
[58] M. Stolterfoht, P. Caprioglio, C.M. Wolff, J.A. Márquez, J. Nordmann, S. Zhang, D. Rothhardt, U. Hörmann, Y. Amir, A. Redinger, L. Kegelmann, F. Zu, S. Albrecht, N. Koch, T. Kirchartz, M. Saliba, T. Unold, D. Neher, Energy Environ. Sci., 12 (2019) 2778-2788.
[59] J. Deng, B. Huang, W. Li, L. Zhang, S.Y. Jeong, S. Huang, S. Zhang, F. Wu, X. Xu, G. Zou, H.Y. Woo, Y. Chen, L. Chen, Angew. Chem. Int. Ed., 61 (2022) e202202177.
[60] S.-Y. Chung, Y.-M. Kim, J.-G. Kim, Y.-J. Kim, Nature Physics, 5 (2008) 68-73.
[61] B. Chen, X. Zheng, M. Yang, Y. Zhou, S. Kundu, J. Shi, K. Zhu, S. Priya, Nano Energy, 13 (2015) 582-591.
[62] C.-C. Zhang, Z.-K. Wang, M. Li, Z.-Y. Liu, J.-E. Yang, Y.-G. Yang, X.-Y. Gao, H. Ma, Journal of Materials Chemistry A, 6 (2018) 1161-1170.
[63] S.Y. Yang, J. Seidel, S.J. Byrnes, P. Shafer, C.H. Yang, M.D. Rossell, P. Yu, Y.H. Chu, J.F. Scott, J.W. Ager, 3rd, L.W. Martin, R. Ramesh, Nat Nanotechnol, 5 (2010) 143-147.
[64] J. Huang, J. Yu, Z. Guan, Y. Jiang, Applied Physics Letters, 97 (2010) 143301.
[65] K.S. Nalwa, J.A. Carr, R.C. Mahadevapuram, H.K. Kodali, S. Bose, Y. Chen, J.W. Petrich, B. Ganapathysubramanian, S. Chaudhary, Energy & Environmental Science, 5 (2012) 7042-7049.
[66] B. Yang, Y. Yuan, P. Sharma, S. Poddar, R. Korlacki, S. Ducharme, A. Gruverman, R. Saraf, J. Huang, Adv Mater, 24 (2012) 1455-1460.
[67] K.S. Shin, T.Y. Kim, G.C. Yoon, M.K. Gupta, S.K. Kim, W. Seung, H. Kim, S. Kim, S. Kim, S.W. Kim, Adv Mater, 26 (2014) 5619-5625.

[68] S.C. Baker-Finch, K.R. McIntosh, D. Yan, K.C. Fong, T.C. Kho, J. Appl. Phys., 116 (2014) 063106.
[69] D. Yan, A. Cuevas, J. Appl. Phys., 114 (2013) 044508.
[70] C. Battaglia, A. Cuevas, S. De Wolf, Energy Environ. Sci., 9 (2016) 1552-1576.
[71] Q. Chen, C. Wang, Y. Li, L. Chen, J Am Chem Soc, 142 (2020) 18281-18292.
[72] B. Stadlober, M. Zirkl, M. Irimia-Vladu, Chem Soc Rev, 48 (2019) 1787-1825.
[73] L. Zhu, Q. Wang, Macromolecules, 45 (2012) 2937-2954.
[74] S. Bae, S. Kim, S.W. Lee, K.J. Cho, S. Park, S. Lee, Y. Kang, H.S. Lee, D. Kim, J Phys Chem Lett, 7 (2016) 3091-3096.
[75] W. Chen, S. Liu, Q. Li, Q. Cheng, B. He, Z. Hu, Y. Shen, H. Chen, G. Xu, X. Ou, H. Yang, J. Xi, Y. Li, Y. Li, Adv Mater, 34 (2022) e2110482.
[76] B. Jeong, L. Veith, T. Smolders, M.J. Wolf, K. Asadi, Adv Mater, 33 (2021) e2100486.
[77] M. Li, H.J. Wondergem, M.J. Spijkman, K. Asadi, I. Katsouras, P.W. Blom, D.M. de Leeuw, Nat Mater, 12 (2013) 433-438.
[78] C. Ribeiro, C.M. Costa, D.M. Correia, J. Nunes-Pereira, J. Oliveira, P. Martins, R. Goncalves, V.F. Cardoso, S. Lanceros-Mendez, Nat Protoc, 13 (2018) 681-704.
[79] Q. Li, W. Ke, T. Chang, Z. Hu, Journal of Materials Chemistry C, 7 (2019) 1532-1543.
[80] T. Leijtens, E.T. Hoke, G. Grancini, D.J. Slotcavage, G.E. Eperon, J.M. Ball, M. De Bastiani, A.R. Bowring, N. Martino, K. Wojciechowski, M.D. McGehee, H.J. Snaith, A. Petrozza, Advanced Energy Materials, 5 (2015) 1500962.
[81] E. Jia, D. Wei, P. Cui, J. Ji, H. Huang, H. Jiang, S. Dou, M. Li, C. Zhou, W. Wang, Adv Sci (Weinh), 6 (2019) 1900252.
[82] J. Duan, M. Wang, Y. Wang, J. Zhang, Q. Guo, Q. Zhang, Y. Duan, Q. Tang, ACS Energy Letters, 6 (2021) 2336-2342.
[83] C. Cho, Y.W. Jang, S. Lee, Y. Vaynzof, M. Choi, J.H. Noh, K. Leo, Sci Adv, 7 (2021) eabj1363.
[84] M. Jeong, I.W. Choi, E.M. Go, Y. Cho, M. Kim, B. Lee, S. Jeong, Y. Jo, H.W. Choi, J. Lee, J.H. Bae, S.K. Kwak, D.S. Kim, C. Yang, Science, 369 (2020) 1615-1620.
[85] W. Zhao, H. Lin, Y. Li, D. Wang, J. Wang, Z. Liu, N. Yuan, J. Ding, Q. Wang, S. Liu, Advanced Functional Materials, 32 (2022) 2112032.
[86] J. Jeong, M. Kim, J. Seo, H. Lu, P. Ahlawat, A. Mishra, Y. Yang, M.A. Hope, F.T. Eickemeyer, M. Kim, Y.J. Yoon, I.W. Choi, B.P. Darwich, S.J. Choi, Y. Jo, J.H. Lee, B. Walker, S.M. Zakeeruddin, L. Emsley, U. Rothlisberger, A. Hagfeldt, D.S. Kim, M. Gratzel, J.Y. Kim, Nature, 592 (2021) 381-385.
[87] G.M. Kim, H. Sato, Y. Ohkura, A. Ishii, T. Miyasaka, Advanced Energy Materials, 12 (2021) 2102856.
[88] Y. Dong, W. Shen, W. Dong, C. Bai, J. Zhao, Y. Zhou, F. Huang, Y.B. Cheng, J. Zhong, Advanced Energy Materials, 12 (2022) 2200417.
[89] Q. Jiang, Y. Zhao, X. Zhang, X. Yang, Y. Chen, Z. Chu, Q. Ye, X. Li, Z. Yin, J. You, Nature Photonics, 13 (2019) 460-466.
[90] Y. Zong, Y. Zhou, Y. Zhang, Z. Li, L. Zhang, M.-G. Ju, M. Chen, S. Pang, X.C. Zeng, N.P. Padture, Chem, 4 (2018) 1404-1415.
[91] Q. Chang, F. Wang, W. Xu, A. Wang, Y. Liu, J. Wang, Y. Yun, S. Gao, K. Xiao, L. Zhang, L. Wang, J. Wang, W. Huang, T. Qin, Angew Chem Int Ed Engl, 60 (2021) 25567-25574.

[92] X. Yang, Y. Ni, Y. Zhang, Y. Wang, W. Yang, D. Luo, Y. Tu, Q. Gong, H. Yu, R. Zhu, ACS Energy Letters, 6 (2021) 2404-2412.
[93] V. Sarritzu, N. Sestu, D. Marongiu, X. Chang, S. Masi, A. Rizzo, S. Colella, F. Quochi, M. Saba, A. Mura, G. Bongiovanni, Sci Rep, 7 (2017) 44629.
[94] J. Chen, N.G. Park, Adv Mater, 31 (2019) e1803019.
[95] R. Sun, Q. Tian, M. Li, H. Wang, J. Chang, W. Xu, Z. Li, Y. Pan, F. Wang, T. Qin, Advanced Functional Materials, 33 (2022) 2210071.
[96] S. Cacovich, G. Vidon, M. Degani, M. Legrand, L. Gouda, J.-B. Puel, Y. Vaynzof, J.-F. Guillemoles, D. Ory, G. Grancini, Nat. Commun., 13 (2022) 2868.
[97] G.-J.A.H. Wetzelaer, M. Scheepers, A.M. Sempere, C. Momblona, J. Ávila, H.J. Bolink, Adv. Mater., 27 (2015) 1837-1841.
[98] M. Zhang, Q. Chen, R. Xue, Y. Zhan, C. Wang, J. Lai, J. Yang, H. Lin, J. Yao, Y. Li, L. Chen, Y. Li, Nat. Commun., 10 (2019) 4593.
[99] B. Chen, S. Wang, X. Zhang, W. Zhu, Z. Cao, F. Hao, Chem. Eng. J., 445 (2022) 136769.
[100] J. Zhang, Y. Sun, C. Huang, B. Yu, H. Yu, Adv. Energy Mater., 12 (2022) 2202542.
[101] X.L. Xu, L.B. Xiao, J. Zhao, B.K. Pan, J. Li, W.Q. Liao, R.G. Xiong, G.F. Zou, Angewandte Chemie, 132 (2020) 20149-20157.
[102] T. Choi, S. Lee, Y.J. Choi, V. Kiryukhin, S.W. Cheong, Science, 324 (2009) 63-66.
[103] Y. Peng, X. Liu, Z. Sun, C. Ji, L. Li, Z. Wu, S. Wang, Y. Yao, M. Hong, J. Luo, Angew Chem Int Ed Engl, 59 (2020) 3933-3937.
[104] W. Gao, R. Brennan, Y. Hu, M. Wuttig, G. Yuan, E. Quandt, S. Ren, Materials Today, 21 (2018) 771-784.
[105] D.W. Fu, H.L. Cai, Y. Liu, Q. Ye, W. Zhang, Y. Zhang, X.Y. Chen, G. Giovannetti, M. Capone, J. Li, R.G. Xiong, Science, 339 (2013) 425-428.
[106] H.Y. Ye, Y.Y. Tang, P.F. Li, W.Q. Liao, J.X. Gao, X.N. Hua, H. Cai, P.P. Shi, Y.M. You, R.G. Xiong, Science, 361 (2018) 151-155.
[107] W.Q. Liao, D. Zhao, Y.Y. Tang, Y. Zhang, P.F. Li, P.P. Shi, X.G. Chen, Y.M. You, R.G. Xiong, Science, 363 (2019) 1206-1210.
[108] H.Y. Ye, Y. Zhang, D.W. Fu, R.G. Xiong, Angew Chem Int Ed Engl, 53 (2014) 11242-11247.
[109] H.Y. Zhang, Z. Wei, P.F. Li, Y.Y. Tang, W.Q. Liao, H.Y. Ye, H. Cai, R.G. Xiong, Angew Chem Int Ed Engl, 57 (2018) 526-530.
[110] X.L. Xu, L.B. Xiao, J. Zhao, B.K. Pan, J. Li, W.Q. Liao, R.G. Xiong, G.F. Zou, Angew Chem Int Ed Engl, 59 (2020) 19974-19982.
[111] E.A. Alharbi, A.Y. Alyamani, D.J. Kubicki, A.R. Uhl, B.J. Walder, A.Q. Alanazi, J. Luo, A. Burgos-Caminal, A. Albadri, H. Albrithen, M.H. Alotaibi, J.E. Moser, S.M. Zakeeruddin, F. Giordano, L. Emsley, M. Gratzel, Nat Commun, 10 (2019) 3008.
[112] C.K. Yang, W.N. Chen, Y.T. Ding, J. Wang, Y. Rao, W.Q. Liao, Y.Y. Tang, P.F. Li, Z.X. Wang, R.G. Xiong, Adv Mater, 31 (2019) e1808088.
[113] J. Huang, Y. Yuan, Y. Shao, Y. Yan, Nat. Rev. Mater., 2 (2017) 1-19.
[114] M. Ahmadi, T. Wu, B. Hu, Adv. Mater., 29 (2017) 1605242.
[115] Y. Yuan, Z. Xiao, B. Yang, J. Huang, J. Mater. Chem. A, 2 (2014) 6027-6041.
[116] S. Shahrokhi, W. Gao, Y. Wang, P.R. Anandan, M.Z. Rahaman, S. Singh, D. Wang, C. Cazorla, G. Yuan, J.M. Liu, T. Wu, Small Methods, 4 (2020) 2000149.

[117] S.B. Jo, M. Kim, D.H. Sin, J. Lee, H.G. Kim, H. Ko, K. Cho, Advanced Energy Materials, 5 (2015).
[118] Z. Xiao, Q. Dong, P. Sharma, Y. Yuan, B. Mao, W. Tian, A. Gruverman, J. Huang, Advanced Energy Materials, 3 (2013) 1581-1588.
[119] C. Sun, Y. Guo, B. Fang, J. Yang, B. Qin, H. Duan, Y. Chen, H. Li, H. Liu, The Journal of Physical Chemistry C, 120 (2016) 12980-12988.
[120] S. Zhang, Y. Lu, B. Lin, Y. Zhu, K. Zhang, N.-Y. Yuan, J.-N. Ding, B. Fang, Solar Energy Materials and Solar Cells, 170 (2017) 178-186.
[121] T. Tiedje, Appl. Phys. Lett., 40 (1982) 627-629.
[122] U. Rau, J.H. Werner, Appl. Phys. Lett., 84 (2004) 3735-3737.
[123] U. Rau, U.W. Paetzold, T. Kirchartz, Physical Review B, 90 (2014) 035211.
[124] B. Qi, J. Wang, J. Mater. Chem., 22 (2012) 24315-24325.
[125] J.C. Blakesley, D. Neher, Physical Review B, 84 (2011) 075210.
[126] Z. Guo, A.K. Jena, G.M. Kim, T. Miyasaka, Energy Environ. Sci., 15 (2022) 3171-3222.

Figure caption

Fig. 1: (a) Structure and Schematic fabrication process of the flexible ZnO-based perovskite solar cell. (b) Schematics and energy-band diagrams of piezo-phototronic effect on the ZnO-based perovskite solar cell. (c) The performance of device under continuous static tensile strains.

Fig. 2: (a) Schematic of perovskite/ZnO single micro/nanowire solar cells, measurement set-up of cells, energy band diagrams of piezo-phototronic effect on cells. (b) Dependence of performance, the open circuit voltage and the short circuit current of device under compressive strain.

Fig. 3: (a) The external electric field poling process of PSCs. (b) The PCE in the condition of ferroelectric polymer doping, only external electric field treatment and the ferroelectric polymer polarization. (c) The photovoltaic performance under different external electric field poling, and the surface potential patterns at the interface of perovskite and TiO_2 layers.

Fig. 4: (a) The potential of perovskite layer measured by KPFM. (b) The mechanism of polarization of PVDF:DH enhancing built-in field. (c) The change of PCE and V_{OC} of device induced by polarization of PVDF:DH.

Fig. 5: Photovoltaic performance of PSCs based on PSCs and PVDF-based PSCs.

Fig. 6: (a) The device structures of PSCs and schematic of ideal exciton dissociation process after electric field poling. (b) AFM morphology and the corresponding surface CPD at the interfaces of TiO_2 and perovskite layers. (c) The performance of molecular ferroelectric polymers doped PSCs with different electric field poling.

Fig. 7: (a) The influence of the electric field poling process on performance of device with 2 wt% P(VDF-TrFE). (b) The statistic parameters of the solar cell performance. (c) Schematic and band diagram in P(VDF-TrFE) doped solar cells under different poling conditions.

Fig. 8: (a) The potential distribution map of the cross-section of the p-i-n structured perovskite solar cells under dark and light illumination conditions. (b) The band alignment of the solar cells before contact, under dark conditions, and under light illumination. (c) The schematic diagram of energy bands for solar cells under the conditions of positive poling and negative poling.

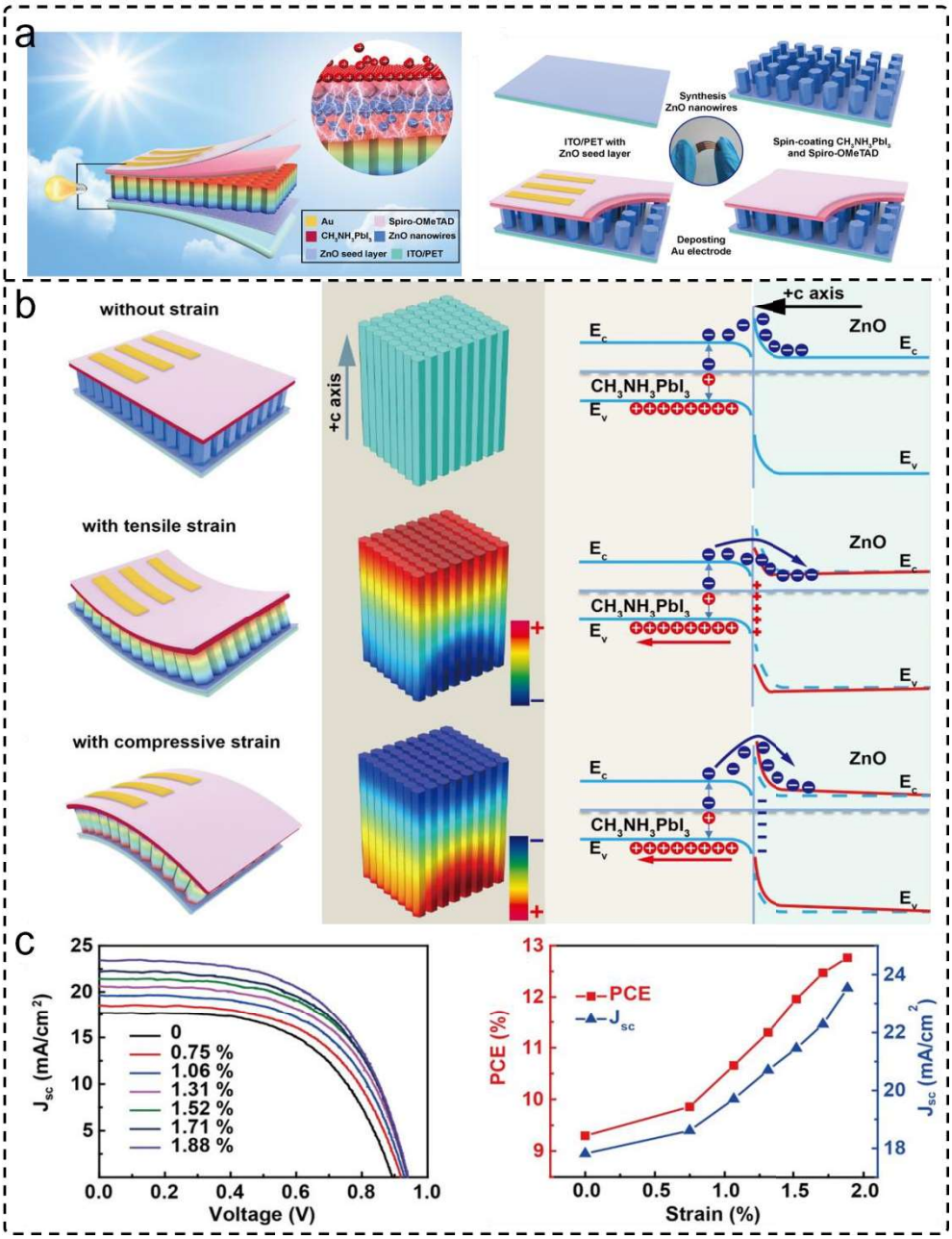
a
Au
Spiro-OMeTAD
CH3NH3PbI3
ZnO nanowires
ZnO seed layer
ITO/PET
Synthesis ZnO nanowires
ITO/PET with ZnO seed layer
Spin-coating CH3NH3PbI3 and Spiro-OMeTAD
Deposting Au electrode
b
without strain
with tensile strain
with compressive strain
+c axis
ZnO
CH3NH3PbI3
Ec
Ev
c
Jsc (mA/cm2)
Voltage (V)
0
0.75 %
1.06 %
1.31 %
1.52 %
1.71 %
1.88 %
PCE (%)
Jsc (mA/cm2)
Strain (%)

Fig. 1

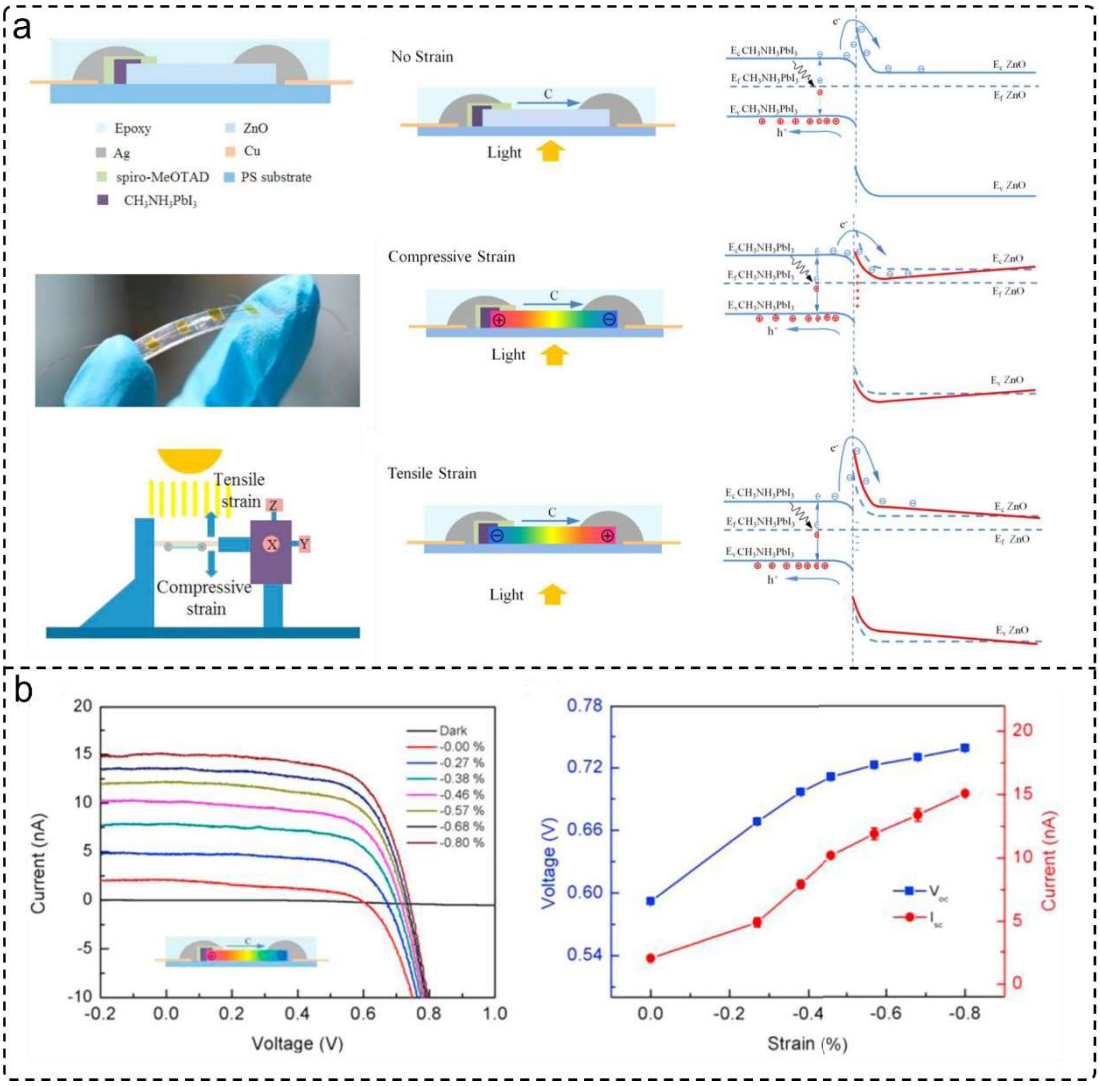
a
Epoxy
ZnO
Ag
Cu
spiro-MeOTAD
PS substrate
$CH_3NH_3PbI_3$
No Strain
Light
Compressive Strain
Light
Tensile strain
Compressive strain
Tensile Strain
Light
b
Dark
-0.00 %
-0.27 %
-0.38 %
-0.46 %
-0.57 %
-0.68 %
-0.80 %
Current (nA)
Voltage (V)
Voltage (V)
Current (nA)
Strain (%)

Fig. 2

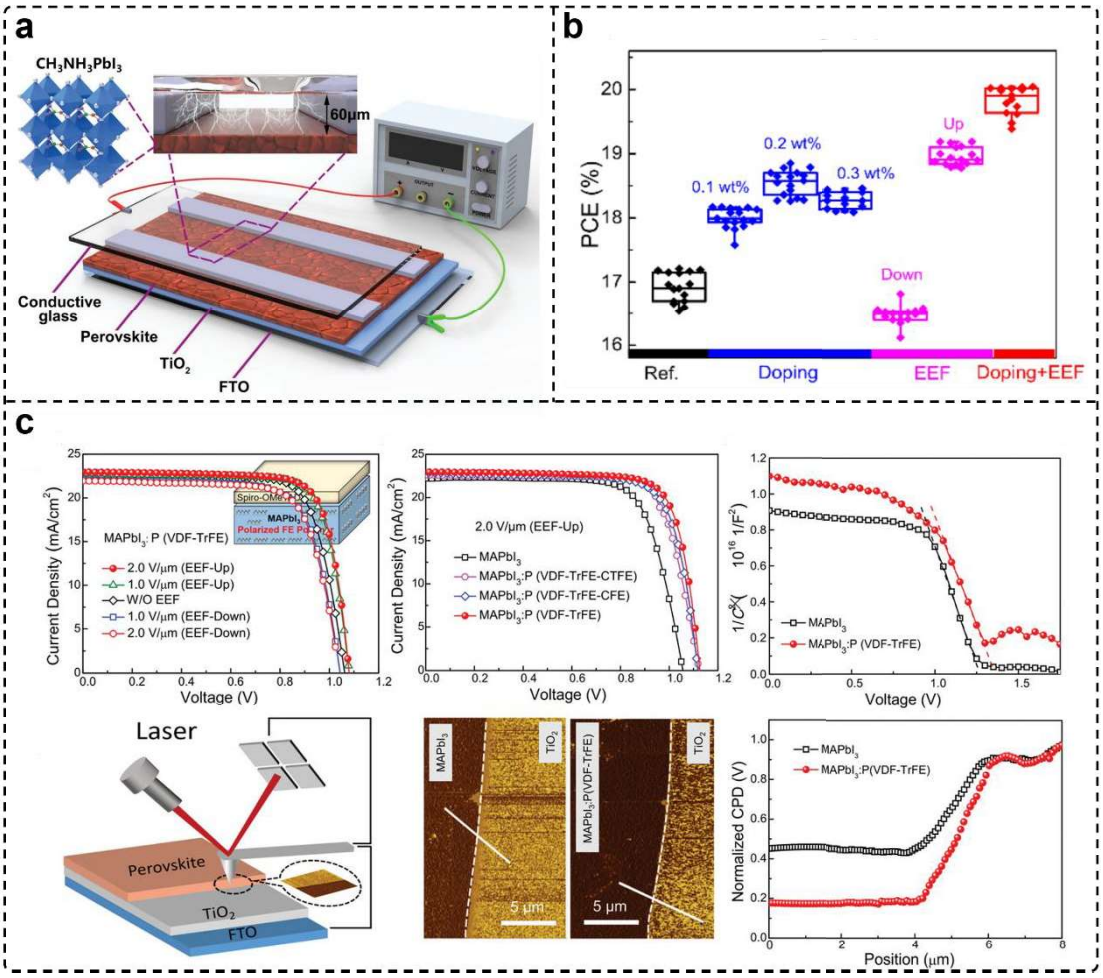
a
$CH_3NH_3PbI_3$
60μm
Conductive glass
Perovskite
TiO_2
FTO
b
PCE (%)
0.1 wt%
0.2 wt%
0.3 wt%
Up
Down
Ref.
Doping
EEF
Doping+EEF
c
Current Density (mA/cm²)
Voltage (V)
MAPbI3:P (VDF-TrFE)
2.0 V/μm (EEF-Up)
1.0 V/μm (EEF-Up)
W/O EEF
1.0 V/μm (EEF-Down)
2.0 V/μm (EEF-Down)
MAPbI3:P (VDF-TrFE-CTFE)
MAPbI3:P (VDF-TrFE-CFE)
MAPbI3
MAPbI3:P (VDF-TrFE)
Laser
Perovskite
TiO2
FTO
5 μm
Normalized CPD (V)
Position (μm)

Fig. 3

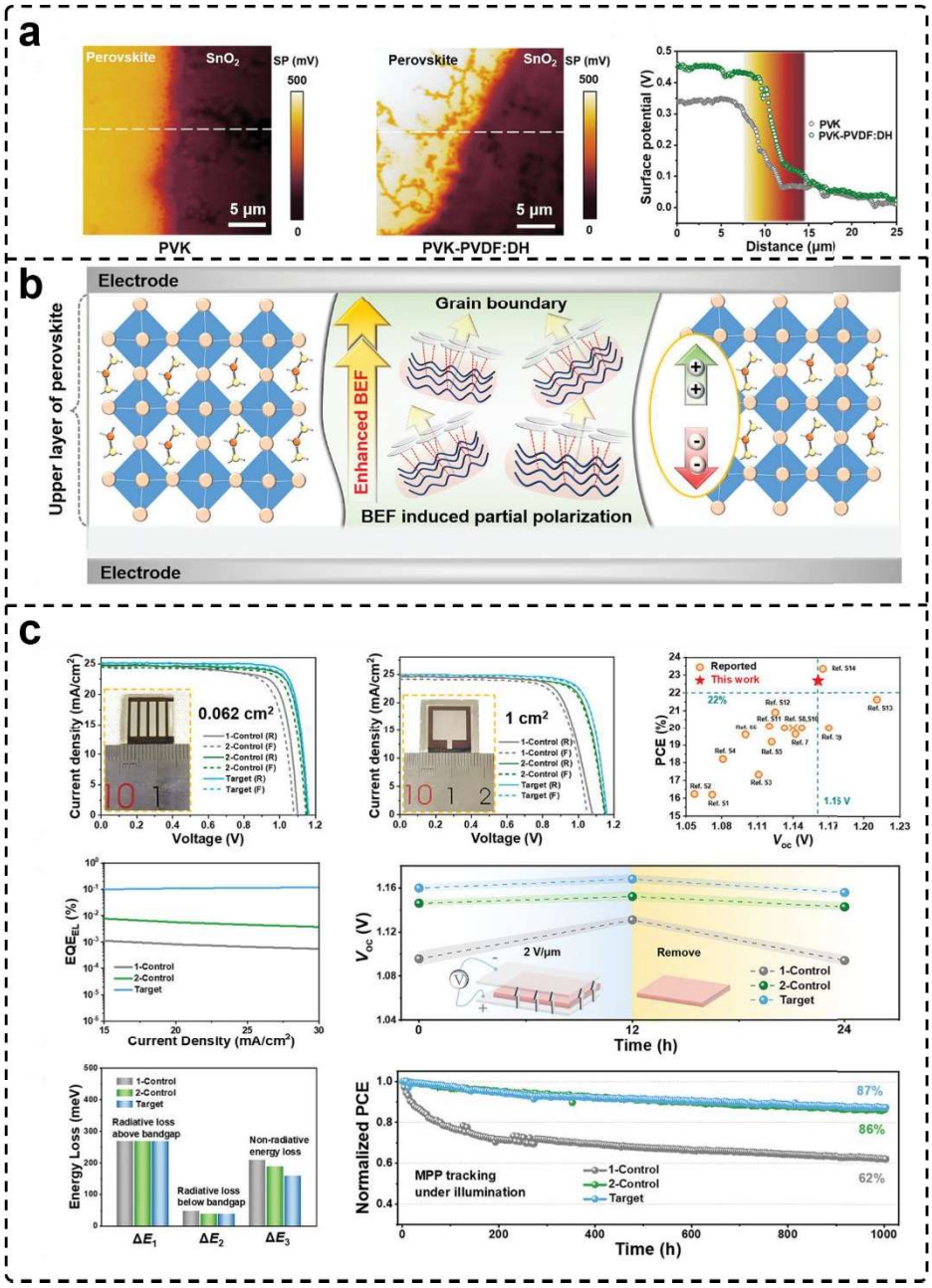
a
Perovskite
SnO2
SP (mV)
500
0
5 μm
PVK
PVK-PVDF:DH
Surface potential (V)
Distance (μm)
b
Electrode
Upper layer of perovskite
Grain boundary
Enhanced BEF
BEF induced partial polarization
c
0.062 cm2
1 cm2
Current density (mA/cm2)
Voltage (V)
Reported
This work
PCE (%)
Voc (V)
EQEEL (%)
Current Density (mA/cm2)
2 V/μm
Remove
Time (h)
Energy Loss (meV)
Radiative loss above bandgap
Radiative loss below bandgap
Non-radiative energy loss
Normalized PCE
MPP tracking under illumination
87%
86%
62%

Fig. 4

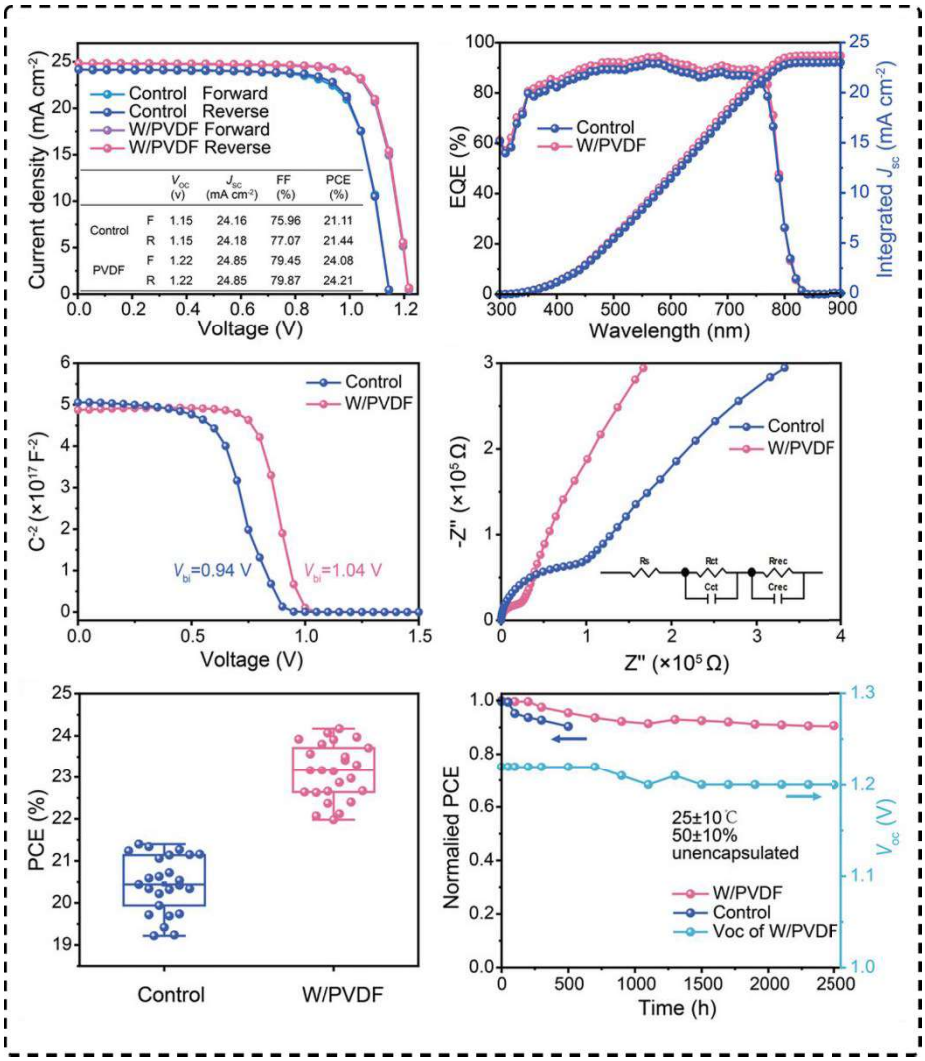
Control Forward
Control Reverse
W/PVDF Forward
W/PVDF Reverse
Current density (mA cm-2)
Voltage (V)
Control F 1.15 24.16 75.96 21.11
Control R 1.15 24.18 77.07 21.44
PVDF F 1.22 24.85 79.45 24.08
PVDF R 1.22 24.85 79.87 24.21
EQE (%)
Integrated Jsc (mA cm-2)
Wavelength (nm)
Control
W/PVDF
C-2 (×10^17 F-2)
Vbi=0.94 V
Vbi=1.04 V
-Z'' (×10^5 Ω)
Z'' (×10^5 Ω)
Rs
Rct
Rrec
Cct
Crec
PCE (%)
Control
W/PVDF
Normalied PCE
25±10℃
50±10%
unencapsulated
Voc of W/PVDF
Voc (V)
Time (h)

Fig. 5

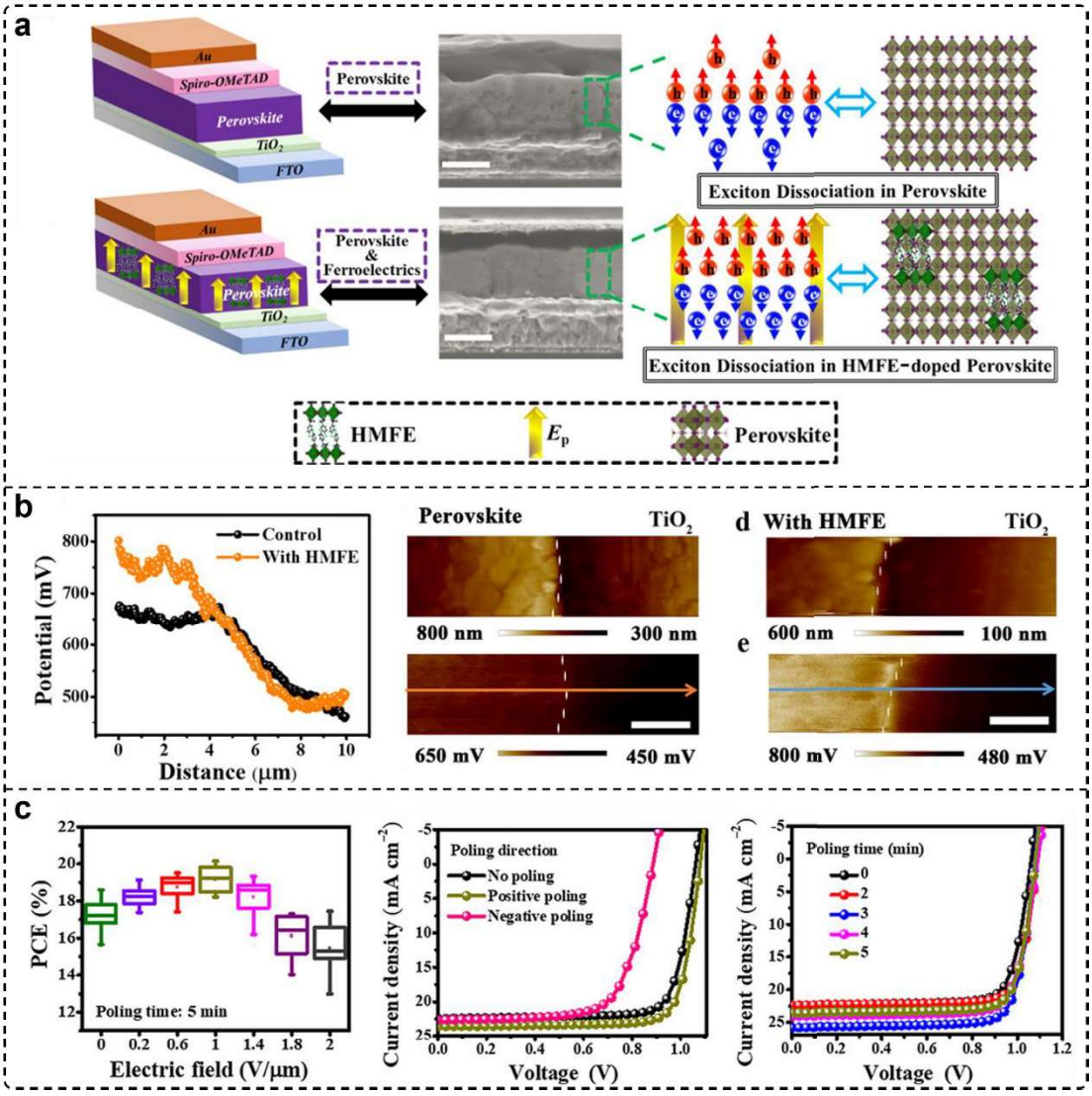
a
Au
Spiro-OMeTAD
Perovskite
TiO2
FTO
Perovskite
Perovskite & Ferroelectrics
Exciton Dissociation in Perovskite
Exciton Dissociation in HMFE-doped Perovskite
HMFE
Ep
Perovskite
b
Control
With HMFE
Potential (mV)
Distance (μm)
Perovskite
TiO2
800 nm
300 nm
650 mV
450 mV
d With HMFE
TiO2
600 nm
100 nm
e
800 mV
480 mV
c
PCE (%)
Poling time: 5 min
Electric field (V/μm)
Poling direction
No poling
Positive poling
Negative poling
Current density (mA cm-2)
Voltage (V)
Poling time (min)
0
2
3
4
5
Current density (mA cm-2)
Voltage (V)

Fig. 6

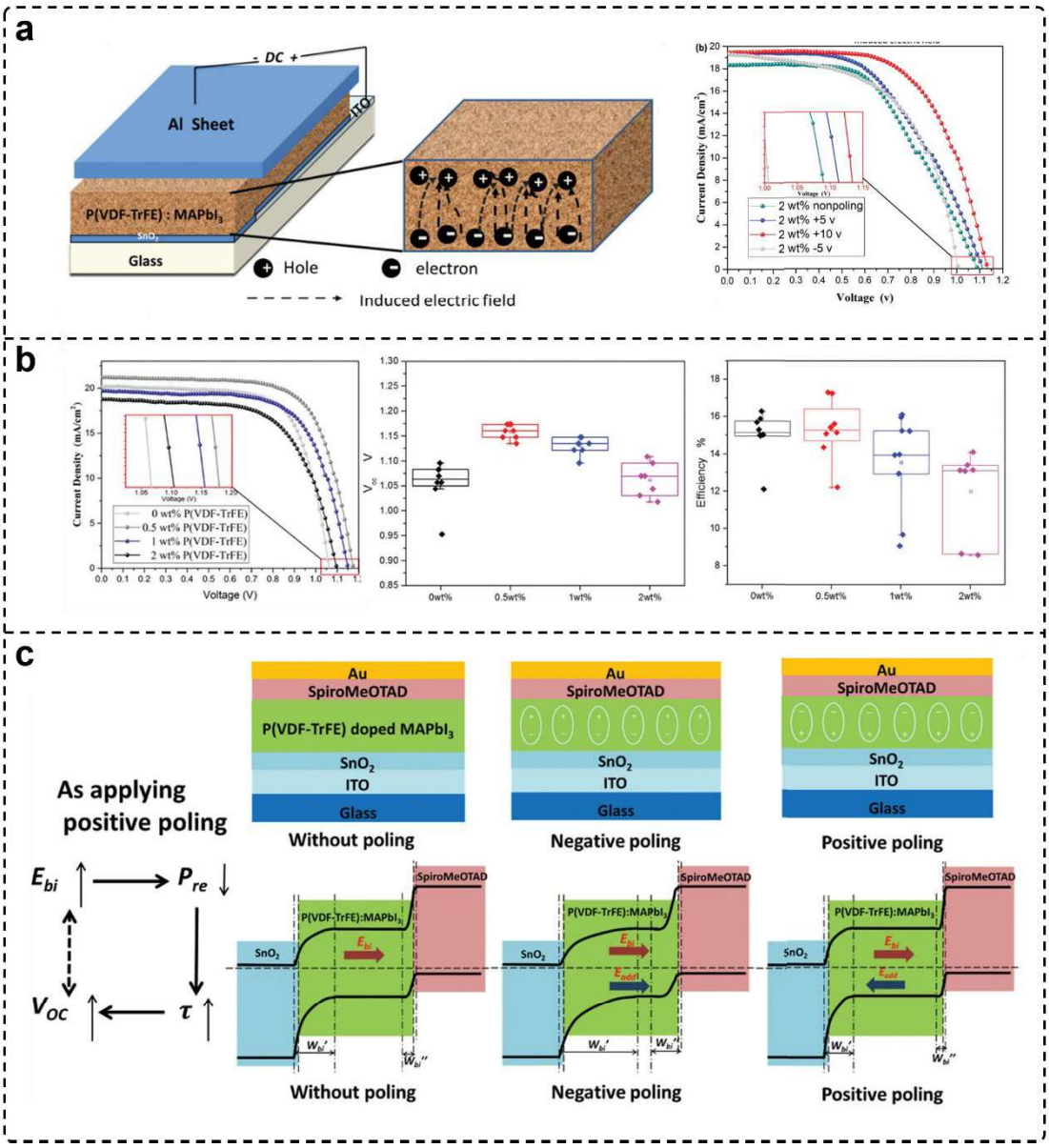
a
- DC +
Al Sheet
ITO
P(VDF-TrFE) : MAPbI3
SnO2
Glass
Hole
electron
Induced electric field
2 wt% nonpoling
2 wt% +5 v
2 wt% +10 v
2 wt% -5 v
Current Density (mA/cm2)
Voltage (v)
b
0 wt% P(VDF-TrFE)
0.5 wt% P(VDF-TrFE)
1 wt% P(VDF-TrFE)
2 wt% P(VDF-TrFE)
Current Density (mA/cm2)
Voltage (V)
Voc V
Efficiency %
0wt%
0.5wt%
1wt%
2wt%
c
As applying positive poling
Ebi
Pre
Voc
τ
Au
SpiroMeOTAD
P(VDF-TrFE) doped MAPbI3
SnO2
ITO
Glass
Without poling
Negative poling
Positive poling
P(VDF-TrFE):MAPbI3
Ebi
Eadd
Wbi'
Wbi''

Fig. 7

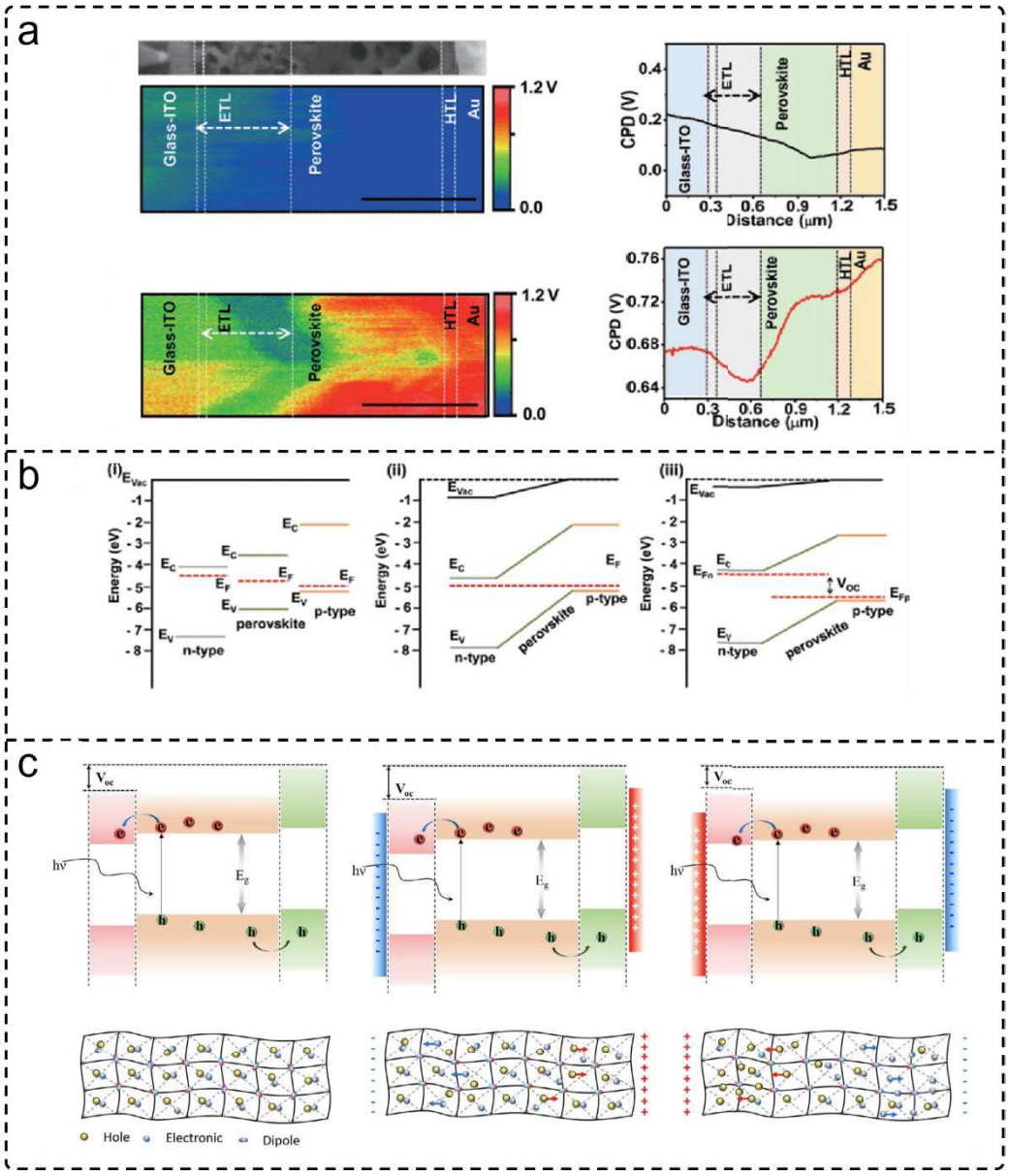
a
Glass-ITO
ETL
Perovskite
HTL
Au
1.2 V
0.0
CPD (V)
Distance (μm)
b
(i)
(ii)
(iii)
Energy (eV)
n-type
perovskite
p-type
c
hν
Hole
Electronic
Dipole

Fig. 8